The electric field gradient for single indium atoms on low-index silver surfaces

1989 J. Phys.: Condens. Matter 1 7407

(http://iopscience.iop.org/0953-8984/1/40/014)

J. Phys.: Condens. Matter **1** (1989) 7407–7418. Printed in the UK

The electric field gradient for single indium atoms on low-index silver surfaces

R Wesche, R Fink, T Klas, G Krausch, R Platzer, J Voigt and G Schatz
Fakultät für Physik, Universität Konstanz, D-7750 Konstanz,
Federal Republic of Germany

Received 16 February 1989

Abstract. The perturbed $\gamma\gamma$ angular correlation (PAC) method has been applied to study isolated ^{111}In atoms on low index silver surfaces. Strong, axial-symmetric electric field gradients are observed on the highly symmetric (111) and (100) surfaces, whereas a non-axial-symmetric field gradient is found for the (110) orientation. Strength and symmetry of the electric field gradients have been studied as a function of measurement temperature. The influence of impurities on the field gradient distributions is discussed. Finally, a comprehensive comparison is given to results reported previously for ^{111}In on the respective copper surfaces. The observed behaviour reflects well known features of the bulk metals.

1. Introduction

The number of experimental techniques for surface characterisation and for the study of processes on surfaces is steadily increasing. One very recent addition to this spectrum of methods is the use of energy splittings of nuclear levels due to the electric or magnetic hyperfine fields produced in atoms which are situated on or near surfaces. In particular, the perturbed $\gamma\gamma$ angular correlation (PAC) method, sensing the electric field gradient at the probe-nuclear site, has proven to be a powerful technique for identifying the position of isolated or embedded impurity atoms and following dynamic phenomena such as diffusion on a microscopic level.

The electric field gradient acting on the probe nucleus is a very short-range quantity produced by extra-nuclear charges and thus yields information about the probe-atomic microscopic surrounding on the surface. First experimental results were reported for ^{111}In on epitaxially grown indium films [1]; however, the most comprehensive study has been carried out for ^{111}In on various low-index and stepped copper single-crystal surfaces [2, 3]. It was shown that after sufficient annealing of the surface most of the probe atoms occupy substitutional sites within the first monolayer. The corresponding electric field gradients are characterised by distinct parameters for the different surface orientations, clearly reflecting the differences in the atomic arrangement on the respective surfaces. Moreover, from the temperature dependence of the electric field gradients insight could be gained in the vibrational behaviour of the surface atoms.

Besides that, a variety of different field-gradient situations has been observed at low temperatures. In case of impurity contamination of the surface, each field-gradient signal corresponds to a well defined probe site or is related to distinct probe-impurity

0953-8984/89/407407 + 12 $02.50

configurations. Strength, symmetry and orientation of the observed electric field gradients not only allow site assignments for the radioactive probes, but also, through the observation of thermal conversion between different probe sites, diffusion data become accessible for various microscopic diffusion paths. In the case of copper, different diffusion processes have been studied, such as step-correlated diffusion, bulk diffusion and surface segregation as well as impurity diffusion on the surface [4].

In this paper we want to report on first results for ^{111}In on different low-index silver surfaces. Being a noble metal of the same crystal structure as copper, silver is expected to behave rather similarly to copper and therefore should serve to test the reproducibility and consistency of the results obtained for ^{111}In on copper surfaces critically. Nevertheless, there are characteristic differences between both metals, such as the different lattice constants and the different solubility of In, which should influence the field-gradient situations to be observed. It will be shown that in the case of the terrace field gradients, which appear above room temperature, the results on silver mainly resemble what was found on copper. However, some characteristic differences occur reflecting the respective differences of the bulk materials. The diffusive behaviour at lower temperatures will be discussed elsewhere [5].

2. Experimental details

For the present PAC experiments we use the isomeric nuclear state ($I = \frac{5}{2}$, $T_{1/2} = 84$ ns) intermediate in the 172–247 keV $\gamma\gamma$ cascade in ^{111}Cd, which is populated through the ^{111}In decay ($T_{1/2} = 2.8\,d$). The nuclear quadrupole moment of this state ($Q = +0.83(13)b$) senses the electric field gradient at the probe nuclear site which splits the isomeric nuclear level. As the second spatial derivative of the electric potential, the electric field gradient is a tensor quantity, commonly described in its principal-axis system through the largest component V_{zz} and the asymmetry parameter $\eta = (V_{xx} - V_{yy})/V_{zz}$. In the case of ^{111}Cd, the PAC method enables the observation of three transition frequencies ω_i, uniquely characterising strength and symmetry of the electric-field-gradient tensor:

$$\omega_i = (3/20\hbar)c_i(\eta)eQV_{zz} \qquad i = 1, 2, 3.$$

The parameter $c_i(\eta)$ can be calculated for a given asymmetry parameter η. For axial symmetry, i.e. $\eta = 0$, one obtains $c_1(0) : c_2(0) : c_3(0) = 1 : 2 : 3$. From these frequencies the quadrupole coupling constant conventionally is derived

$$\nu_Q = eQV_{zz}/h.$$

From the relative amplitudes of the transition frequencies information can be gained about the orientation of the field-gradient principal-axis system. (For a detailed description of the method, see [3].)

Silver single crystals have been cut along the three low-index planes, i.e. (111), (100) and (110), respectively. After chemical etching in a mixture of NH_4OH and H_2O_2, the crystals have been cleaned under UHV conditions in a cycle of successive ion sputtering (Ar^+, 600 eV) and heating (850 K). After the final treatment Auger-electron spectra (AES) were taken showing the impurity concentrations to be less than 10^{-2} monolayers (ML). Low energy electron diffraction (LEED) measurements were performed to monitor the surface atomic structure. At 77 K radioactive probe atoms were deposited in situ on to the surface with concentrations of the order of 10^{-4} ML. After annealing the sample, PAC spectra were taken with the sample being positioned in the centre of a five γ-detector arrangement.

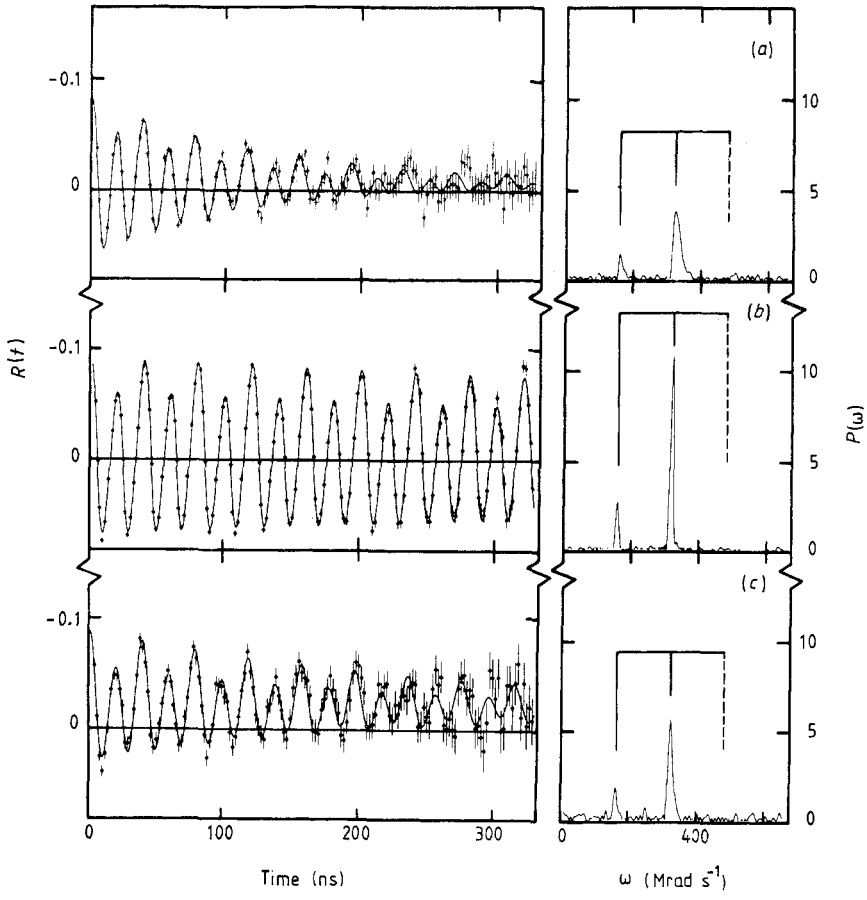

Figure 1. $R(t)$ time spectra and Fourier transforms for ^{111}In on Ag(111) for different Cl contaminations and annealing temperatures. The damping of the time modulation is smaller for decreasing Cl contamination and increasing annealing temperature. (Due to the chosen sample-detector geometry only the first two transition frequencies are visible.) (*a*) T_A = 250 K, c_{Cl} = 5%; (*b*) T_A = 420 K, c_{Cl} = 2%; (*c*) T_A = 470 K, c_{Cl} = 6%.

3. Results and discussion

3.1. Electric field gradients for ^{111}In on terrace sites

3.1.1. ^{111}In on Ag(111). A silver single-crystal surface was prepared with the surface normal pointing within ±1° along the ⟨111⟩ direction. With the depositon of the ^{111}In probe atoms at 77 K some Cl impurities were carried in ($c_{Cl} < 5 \times 10^{-2}$ ML).

In figure 1(*a*) and (*b*) PAC spectra are shown, which were recorded at 77 K after annealing the sample for 10 min at 250 K and 420 K, respectively. The Fourier transforms clearly show two well defined transition frequencies; the third frequency cannot be observed because of the chosen sample-detector geometry. From the relative magnitudes of the transition frequencies an asymmetry parameter $\eta = 0.00(5)$ is deduced. The amplitudes of the two frequencies suggest that the z-principal axis of the electric-field-gradient tensor is oriented along the ⟨111⟩ direction; additional experiments with

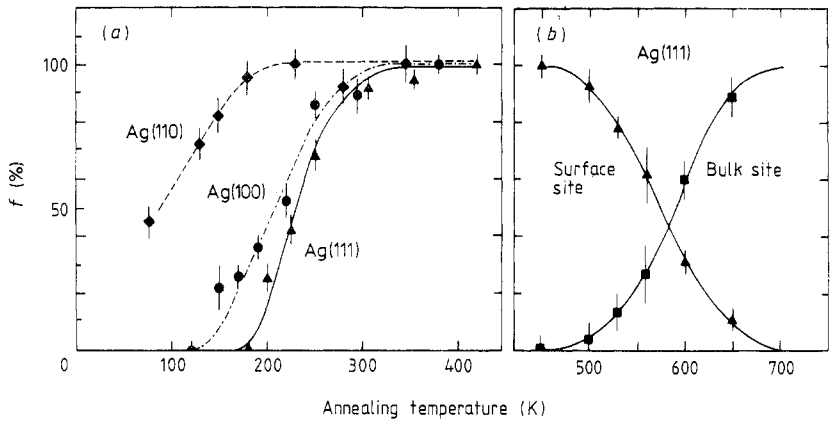

Figure 2. (*a*) Fraction of probe atoms experiencing terrace field gradients as a function of annealing temperature for the three low-index Ag surfaces. (*b*) Behaviour of ^{111}In on Ag(111) at elevated annealing temperatures. While the surface signal is continuously decreasing above 500 K, an increasing fraction of probe atoms migrates into bulk and occupies regular lattice sites, resulting in a vanishing electric field gradient.

different sample–detector geometries clearly confirm this result. Obviously, after sufficient annealing most of the probe atoms experience a unique axial-symmetric electric field gradient with its symmetry axis pointing perpendicular to the (111) plane. In particular, this field gradient is characterised by the following parameters (T_M = 77 K): $|V_{zz}| = 8.6(13) \times 10^{17}$ V cm^{-2}, $\eta = 0.00(5)$, z-principal axis normal to (111) plane.

The high symmetry as well as the orientation of the observed electric field gradient is only compatible with probe sites of high rotational symmetry about the surface normal, i.e. either adatomic sites or substitutional sites within the first monolayer. As shown in figure 2, the first possibility can be ruled out by the annealing behaviour observed. One would expect at least a small fraction of probe atoms to occupy adatomic sites directly after deposition at 77 K. However, only after annealing the surface to about room temperature are the respective probe sites populated, leading to the observed axial-symmetric field gradient.

The same behaviour has been found for ^{111}In on Cu(111) [4]. Additional experiments on stepped Cu(111) surfaces revealed a step-correlated diffusion process of the probe atoms at low temperatures, finally leading to the population of substitutional sites within the first monolayer. In addition, field-gradient calculations by Lindgren [6] resulted in quite different electric field gradients for ^{111}Cd in adatomic and substitutional terrace sites on Cu(111), strongly supporting the assumption of substitutional terrace sites, too.

Comparing the two PAC spectra in figure 1(*a*) and (*b*) it can be seen that after annealing the surface to 420 K the transition-frequency distribution is narrower, i.e. the electric-field-gradient situation is more uniform at the probe-atom ensemble. At the same time a quantitative decrease of the Cl contamination on the surface with increasing annealing temperature was observed via AES. In figure 1(*c*) a PAC spectrum is shown from a different experiment, where the Cl concentration amounted to 6×10^{-2} ML even after annealing up to 470 K. Again a rather broad field-gradient distribution is observed, resulting in a damping of the modulation in the $R(t)$ time spectrum. From this information it can be concluded that Cl atoms in the vicinity of the probe atoms slightly alter

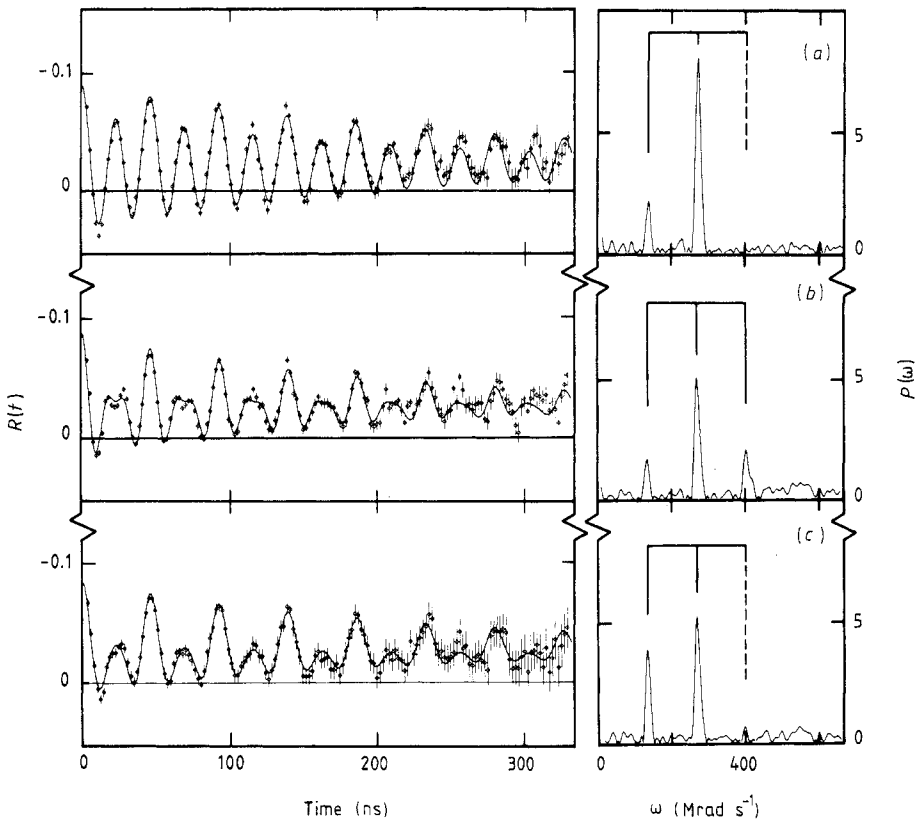

Figure 3. $R(t)$ time spectra, evaluated for different γ-detector combinations, and corresponding Fourier transforms for ^{111}In on Ag(100). The surface normal is placed in the plane of four γ-detectors pointing under 45° between two adjacent detectors. (*a*) Conventional $R(t)$ using the four γ-detectors in a plane. (*b*) $R(t)$ including the fifth γ-detector, which is positioned perpendicular to the four-detector plane and acts as a start detector. (*c*) As for (*b*), but with the fifth γ-detector acting as stop detector.

the electric field gradient, thus leading to a broadening of the transition-frequency distribution.

As indicated in figure 2, at annealing temperatures above 500 K an increasing fraction of probe atoms experiences a vanishing electric field gradient, as is expected for probe atoms on lattice sites with cubic symmetry. At the same time the fraction of probe atoms on terrace sites decreases, clearly showing the onset of diffusion into bulk and the population of bulk lattice sites by the indium atoms.

3.1.2. ^{111}In on Ag(100). Similar experiments as described above have been performed for Ag(100) surfaces. Figure 3 shows different counting-rate ratios $R(t)$ and the respective Fourier transforms of a particular sample after annealing up to 380 K.

In contrast to figure 3(*a*), where the same counting-rate ratio was performed as is shown in figure 1, in figure 3(*b*) and (*c*) different detector combinations are chosen for the detection of the two γ-quanta, changing the observed amplitudes of the three transition frequencies. In particular, in figure 3(*b*) the third frequency becomes clearly visible. As in the case of Ag(111) an axial-symmetric electric field gradient is deduced

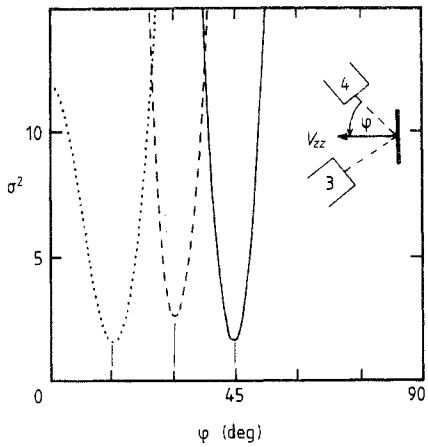

Figure 4. Least-square deviations between theoretical and experimental amplitudes of the transition frequencies for three different sample-detector geometries. The surface normal was pointing under 15°, 30° and 45° between two of the detectors in the four-detector plane. For the calculations, the direction of V_{zz} with respect to the detectors has been varied. The well defined minima show that the z-principal axis of the field-gradient tensor is pointing perpendicular to the (100) plane.

from the magnitudes of the different transition frequencies. Again, the z-principal axis is found to point along the surface normal (T_M = 77 K): $|V_{zz}| = 7.5(11) \times 10^{17}$ V cm^{-2}, $\eta = 0.00(5)$, z-principal axis normal to (100) plane.

In order to elucidate the quality of the results obtained for the orientation of the electric-field-gradient tensor the least-squares deviations have been computed between the experimental amplitudes of the transition frequencies and calculations of these amplitudes as a function of the field-gradient orientation. Figure 4 shows results of this procedure for three different experiments where the surface normal was pointing under 15°, 30° and 45° with respect to one of the detectors. The well defined minima of the mean-squares deviation σ^2 at the respective angles clearly confirm the fact that the z-principal axis of the field-gradient tensor is pointing along the surface normal within an experimental error of ±3°.

As in the case of Ag(111), different field-gradient situations are observed on Ag(100) directly after deposition of the radioactive probes at 77 K and for low annealing temperatures. As shown in figure 2, only after annealing to 150 K does the fraction of probe atoms experiencing the axial-symmetric field gradient become dominant. Therefore we again assign this unique field gradient to probe atoms on substitutional terrace sites. The high symmetry as well as the field-gradient orientation fit this assignment, clearly reflecting the high symmetry of the respective lattice sites within the (100) terrace.

It is worth mentioning that the transition-frequency distributions in figure 3 are slightly broader than in figure 1(*b*). This observation corresponds to the fact that the surface was contaminated with chlorine during the deposition of the probe atoms ($c_{Cl} < 3 \times 10^{-2}$ ML). In contrast the case of Ag(111), this contamination was not removed by heating the sample but could be observed even after annealing the surface up to 500 K. This correspondence strongly supports the assumption that Cl impurities in the vicinity of the probe atoms are responsible for slight changes of the electric field gradients acting on the probe nuclei.

3.1.3. ^{111}In on Ag(110). The (110) surface has a less symmetric atomic structure and is therefore expected to produce a rather different field-gradient situation compared to the highly symmetric surface orientations discussed above. Figure 5 shows PAC spectra and Fourier transforms of a Ag(110) surface after deposition of the probe atoms and subsequent annealing. The two spectra were recorded at 77 K and 420 K, respectively.

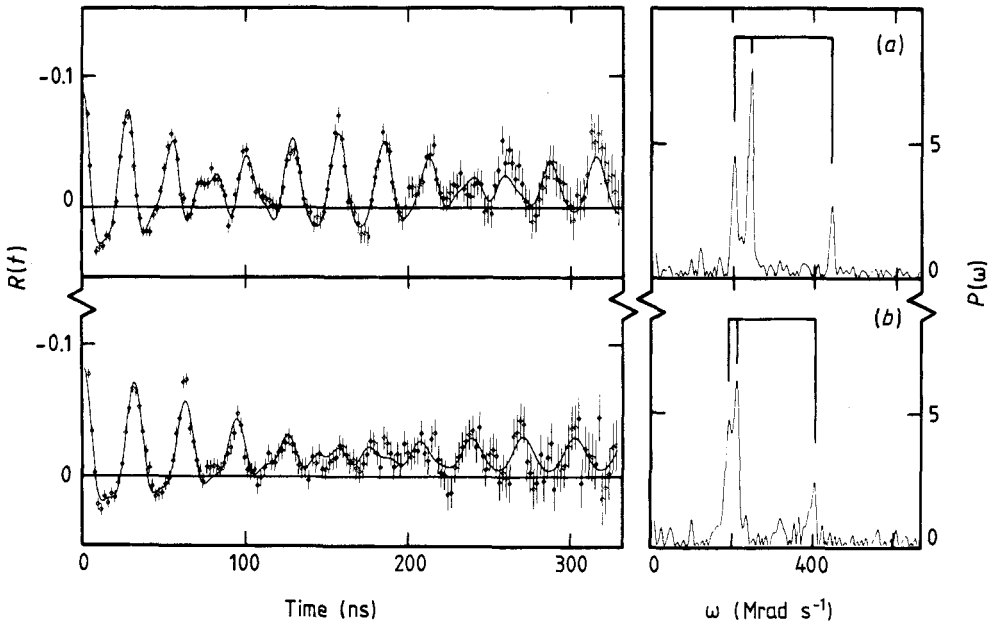

Figure 5. $R(t)$ time spectra and Fourier transforms for ^{111}In on Ag(110) for different measurement temperatures. (*a*) $T_M = 77$ K. The less symmetric structure of the (110) surface leads to a non-axial-symmetric electric field gradient. The first two transition frequencies are close together, indicating a non-zero asymmetry parameter η. (*b*) $T_M = 420$ K. With increasing temperature a small shift of the transition frequencies to lower values can be observed. Moreover, the first two frequencies move even closer together, corresponding to a temperature dependent asymmetry parameter η.

Again, well-defined frequencies occur, characterising a unique electric field gradient. However, in contrast to the spectra shown above, the first two transition frequencies are rather close, indicating a non-zero asymmetry parameter η. For the same reason the third frequency can be seen here, although the same counting-rate ratio was used as is shown in figures 1 and 3(*a*). In particular, the following field-gradient parameters are deduced ($T_M = 77$ K): $|V_{zz}| = 7.0(11) \times 10^{17}$ V cm^{-2}, $\eta = 0.80(1)$.

Other than on the highly symmetric (111) and (100) surfaces on Ag(110) the probe atoms experience a non-axially symmetric electric field gradient. The vanishing axial symmetry leads to a distinction of all three principal axes of the field-gradient tensor. Thus, the orientation of all three axes with respect to the crystallographic axes has to be determined. For that purpose a least-squares fit has been performed as described above, yielding the following orientation of the principal axes system: z-axis normal to (110) plane, y-axis along closest-packed atomic rows (i.e. along $\langle 1\bar{1}0 \rangle$).

This result clearly shows a correlation between the field-gradient orientation and the surface structure. In case of the (110) surface three different probe sites are in agreement with the observed symmetry and orientation of the field gradient: adatomic hollow sites and bridge sites as well as substitutional terrace sites. The annealing behaviour for this field gradient is shown in figure 2. In contrast to the (111) and (100) surfaces, on Ag(110) a measurable fraction of probe atoms experiences the strong, non-axially symmetric field gradient directly after deposition at 77 K. However, further annealing leads to an increase of this fraction, which then remains stable up to about 450 K. We therefore also assume substitutional terrace sites for the probe atoms in the case of Ag(110).

Comparing the annealing behaviour of the terrace field gradients for the different surface orientations, it can be seen that the incorporation of the probe atoms into the first monolayer takes place at different annealing temperatures. The highest temperature is required for the densely packed (111) surface, whereas the population of substitutional terrace sites starts even at 77 K for the rather open (110) structure. This trend may serve as a further indication for the consistency of the chosen site assignments.

The two PAC spectra in figure 5 indicate that with increasing measurement temperature the absolute magnitude of the transition frequencies shifts to lower values. Moreover, the ratio between the first and the second frequency changes, i.e. the asymmetry parameter η is a temperature-dependent quantity, too. This temperature dependence will be discussed in more detail below.

3.2. Temperature dependence of terrace field gradients

It has been shown that, after deposition of probe atoms and subsequent annealing of the samples, unique electric field gradients are found for the individual surface orientations, assigned to probe atoms occupying substitutional terrace sites on the respective surfaces. These terrace field gradients may now be observed within a temperature range of 77–520 K, and their strength and symmetry can be studied as a function of measurement temperature. In case of an isotropic mean-square displacement of the lattice ions a $T^{3/2}$-dependence of the electric field gradient is expected and is observed in many non-cubic bulk metals [7]. However, due to the inherent anisotropy of a crystal surface, a different temperature behaviour for surface field gradients should result. In fact, for ^{111}In on Cu(100) and Cu(111) a linear temperature dependence of the field gradient was found [3], strongly supporting the notion of a two-dimensional phonon spectrum on the surface.

Figure 6 summarises the results obtained for the three low-index silver surfaces. In order to underline the accuracy in the determination of the transition frequencies via the PAC method, in figure 6 the quadrupole coupling constant ν_Q has been plotted rather than the field gradient component V_{zz}. The latter contains a large experimental error due to the uncertainty in the magnitude of the nuclear quadrupole moment.

In case of Ag(111) the temperature dependence of the electric field gradient is rather weak. As shown in figure 6, a least-squares fit approximately reveals a T^2-dependence of the terrace field gradient. However, since the strength of the temperature dependence is very small, a linear or also a $T^{3/2}$-dependence can be fitted to the data almost equally well. In the intermediate temperature range we find a decrease of about $6 \times 10^{-5}\ \mathrm{K}^{-1}$.

For Ag(100) the temperature dependence is slightly stronger and clearly shows a linear behaviour. In particular one finds the following dependence $\nu_Q = 151.3(3)\ \mathrm{MHz}\ (1 - 1.64(6) \times 10^{-4}\ \mathrm{K}^{-1} \times T)$.

The fact that the temperature dependence of the electric field gradient is stronger on the (100) surface than on the (111) surface may be explained by the different atomic densities on the two surface orientations. In fact, the strongest temperature dependence is observed on the (110) surface, which has the most open structure of the surface atoms. The temperature dependence of the field gradient on Ag(110) is definitely non-linear. Assuming a $T^{3/2}$ behaviour one finds $\nu_Q = 141.2(3)\ \mathrm{MHz}\ (1 - 1.55(7) \times 10^{-5}\ \mathrm{K}^{-3/2} \times T^{3/2})$.

Moreover, in case of Ag(110) not only the strength of the field gradient varies with temperature. In addition, as shown in figure 7, a drastic change in the asymmetry parameter η is observed, which increases with increasing temperature up to 420 K. At

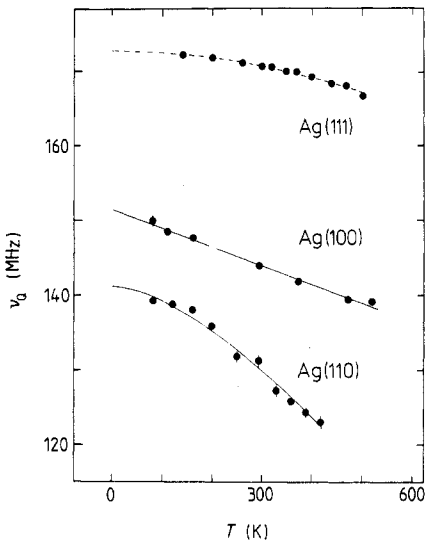

Figure 6. Strength of the terrace field gradient characterised by the quadrupole coupling constant as a function of measurement temperature for the three low index Ag surfaces.

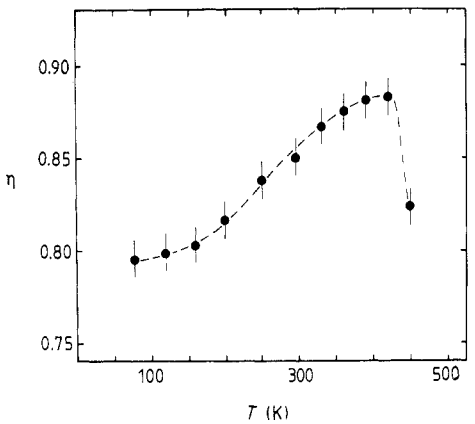

Figure 7. Temperature dependence of the asymmetry parameter η for ^{111}In on Ag(110).

450 K the asymmetry parameter decreases again, at the same time a broadening of the field-gradient distribution is observed. This may be due to slight changes of the atomic positions within the atomic rows, leading to an arrangement of the surface atoms closer to cubic symmetry.

The distance between the first and the second monolayer in (110) orientation is smaller than the bulk value by about 7%. Moreover, different vibrational amplitudes have been observed for the first and second monolayer on Ag(110) [8]. The continuous increase of the asymmetry parameter may thus be the consequence of a temperature-dependent relaxation of the first monolayer. A similar effect on the asymmetry parameter has also been observed on Cu(110) [3].

Comparing the different temperature dependences of the terrace field gradients it becomes clear that the strength of the temperature dependence scales with the atomic densities on the respective surfaces. This fits the expectation that the mean-square displacement of the surface atoms is the larger the more open the surface structure. In the case of the weak temperature dependence on Ag(111) it may be necessary additionally to take into account the thermal expansion of the lattice. This would explain a stronger than linear reduction of the field gradient with increasing temperature. However, as mentioned above the data do not allow an accurate determination of the exponent. The $T^{3/2}$-dependence of the field gradient on the quite open Ag(110) surface suggests that the lateral mean-square displacements already become comparable with the displacements perpendicular to the surface.

3.3. Comparison with the results for ^{111}In on copper surfaces

In table 1 the results are summarised and compared with the results for ^{111}In on copper surfaces as published earlier [2, 3, 4]. On either material the strength of the electric field

Table 1. Terrace field gradients obtained at 77 K for ^{111}In at different silver surfaces (this work) compared to the results for copper surfaces [2, 3].

		Ag	Cu	$\lvert V_{zz,Cu}\rvert/\lvert V_{zz,Ag}\rvert$
(111) surface	ν_Q	172(1) MHz[a]	202(1) MHz	
	$\lvert V_{zz}\rvert$	$8.6(13) \times 10^{17}$ V cm^{-2}	$10.1(14) \times 10^{17}$ V cm^{-2}	1.17(1)
	η	0.00(5)	0.00(5)	
	Orientation	$z \perp$ surface	$z \perp$ surface	
	T-dependence	[b]	Linear	
		$B = 7.7(6) \times 10^{-5}$ K^{-1}	$B = 1.11(3) \times 10^{-4}$ K^{-1}	
(100) surface	ν_Q	150(1) MHz	181(1) MHz	
	$\lvert V_{zz}\rvert$	$7.5(11) \times 10^{17}$ V cm^{-2}	$9.0(14) \times 10^{17}$ V cm^{-2}	1.20(1)
	η	0.00(5)	0.00(5)	
	Orientation	$z \perp$ surface	$z \perp$ surface	
	T-dependence	Linear	Linear	
		$B = 1.64(6) \times 10^{-4}$ K^{-1}	$B = 1.05(4) \times 10^{-4}$ K^{-1}	
(110) surface	ν_Q	141(1) MHz	159(1) MHz	
	$\lvert V_{zz}\rvert$	$7.0(11) \times 10^{17}$ V cm^{-2}	$7.9(12) \times 10^{17}$ V cm^{-2}	1.13(1)
	η	0.80(1)	0.74(1)	
	Orientation	$z \perp$ surface	$z \perp$ surface	
		y along $\langle 1\bar{1}0\rangle$	y along $\langle 1\bar{1}0\rangle$	
	T-dependence	$T^{3/2}$ [c]	$T^{3/2}$	
		$B = 1.55(7) \times 10^{-5}$ K$^{-3/2}$	$B = 0.66(1) \times 10^{-5}$ K$^{-3/2}$	

[a] The experimental error contains small differences in the value of ν_Q occurring between different experiments.
[b] Linear dependence assumed for comparison.
[c] A least-squares fit revealed an exponent of 1.8(3).

gradient decreases as one goes from the densely packed (111) surface to the open (110) surface. The asymmetry parameter η clearly reflects the symmetry of the probe sites on the different surface orientations; on the (110) surface quite similar asymmetry parameters are observed. The temperature dependence of the terrace field gradients shows similar trends as well; in particular, the extraordinary behaviour on the (110) surface has been found on copper, too. This clearly shows that the temperature dependent asymmetry parameter is a characteristic feature of the (110) structure rather than any impurity induced effect or an experimental artifact.

However, comparing the absolute values of the strength of the field gradients, characteristic differences occur, reflecting the different lattice constants of the two metals. In table 1 the ratio $|V_{zz,Cu}|:|V_{zz,Ag}|$ is calculated for the different surface orientations. It is worth mentioning that for all surface orientations this ratio scales approximately with the inverse ratio of the lattice constants ($a_{Ag}:a_{Cu} = 0.409\,nm:0.361\,nm = 1.13$). There is no obvious explanation for that observation; according to a simple point-charge model the strength of the electric field gradient is expected to scale with the third power of the lattice constants rather than linearly.

Further similarities are found concerning the influence of structural imperfections as well as impurities on the width of the field-gradient distributions. It seems to be a general trend that rather high annealing temperatures are needed after deposition of the radioactive probes to observe unique terrace field gradients. Chlorine contamination can be shown to play an important role, leading to a broadening of the transition frequencies, which vanishes only with decreasing Cl concentration.

On the other hand there are differences in the chemical behaviour between the substrate materials and the different impurities, e.g. the indium probe atoms. The most striking difference is seen in the behaviour of the indium probe atoms at elevated annealing temperatures. As shown in figure 2, almost all of the probe atoms were found to migrate into the bulk for Ag(111) at annealing temperatures above 500 K; the same behaviour was also observed for Ag(100) and Ag(110). However, from the Cu(111) and Cu(100) surfaces the majority of the probe atoms is desorbed into vacuum. In the case of Cu(110) the probe atoms start to diffuse into the bulk only at annealing temperatures above 700 K, while surface segregation can be observed at room temperature. These results reflect the fact that indium has a high solubility in silver whereas it is almost unsoluble in copper.

4. Conclusions

In this paper first results for ^{111}In on various low-index Ag surfaces have been reported. It has been shown that after sufficient annealing a vast majority of the probe atoms experiences well defined, unique electric field gradients, which can be attributed to substitutional probe sites within the first monolayer of the respective surfaces. Strength, symmetry and orientation of the field gradients clearly reflect the distinct atomic structures of the different surface orientations investigated. Impurities in the vicinity of the probe atoms as well as surface imperfections have been found to broaden the observed field-gradient distributions. The temperature dependence of the electric field gradients is discussed in the frame of lattice vibrations and has been shown to strongly depend on the atom densities on the different surface orientations.

A systematic study on the silver system can be used as a critical test for the interpretation of the results obtained for ^{111}In on copper surfaces. Additional experiments

have been performed to study the probe-atom diffusion on low-index and stepped silver surfaces at low temperatures, which will be published elsewhere [5]. An extension of our PAC work to other systems (magnetic materials, semiconductors) is in progress and will open new, interesting applications.

Acknowledgments

The assistance of U Wöhrmann and X L Ding during the preparation of this paper is thankfully acknowledged. This work was supported by the Deutsche Forschungsgemeinschaft, Bonn (Sonderforschungsbereich 306).

References

[1] Körner W, Keppner W, Lehndorff-Junges B and Schatz G 1982 *Phys. Rev. Lett.* **49** 1735
[2] Klas T, Voigt J, Keppner W, Wesche R and Schatz G 1986 *Phys. Rev. Lett.* **57** 1068
[3] Klas T, Fink R, Krausch G, Platzer R, Voigt J, Wesche R and Schatz G 1989 *Surf. Sci.* **216** 270
[4] Klas T, Fink R, Krausch G, Platzer R, Voigt J, Wesche R and Schatz G 1988 *Europhys. Lett.* **7** 151
[5] Fink R, Wesche R, Klas T, Krausch G, Platzer R, Voigt J, Wöhrmann U and Schatz G 1989 *Surf. Sci.* at press
[6] Lindgren B 1987 *Hyperfine Interact.* **34** 217
[7] Witthuhn W and Engel W 1983 *Springer Topics in Current Physics* vol 31, ed. J Christiansen (Berlin: Springer) p 205
[8] Holub-Krappe E, Horn K, Frenken J W M, Kraus R L and van der Veen J F 1987 *Surf. Sci.* **188** 335